

Emergent periodic and quasiperiodic lattices on surfaces of synthetic Hall tori and synthetic Hall cylinders

Yangqian Yan,¹ Shao-Liang Zhang,² Sayan Choudhury,¹ and Qi Zhou¹

¹*Department of Physics and Astronomy, Purdue University, West Lafayette, IN, 47907*

²*School of Physics, Huazhong University of Science and Technology, Wuhan 430074, People's Republic of China*

(Dated: January 3, 2020)

Synthetic spaces allow physicists to bypass constraints imposed by certain physical laws in experiments. Here, we show that a synthetic torus, which consists of a ring trap in the real space and internal states of ultracold atoms cyclically coupled by Laguerre-Gaussian Raman beams, could be threaded by a net effective magnetic flux through its surface—an impossible mission in the real space. Such synthetic Hall torus gives rise to a periodic lattice in the real dimension, in which the periodicity of density modulation of atoms fractionalizes that of the Hamiltonian. Correspondingly, the energy spectrum is featured by multiple bands grouping into clusters with nonsymmorphic-symmetry-protected band crossings in each cluster, leading to swaps of wavepackets in Bloch oscillations. Our scheme allows physicists to glue two synthetic Hall tori such that localization may emerge in a quasicrystalline lattice. If the Laguerre-Gaussian Raman beams and ring traps were replaced by linear Raman beams and ordinary traps, a synthetic Hall cylinder could be realized and deliver many of the aforementioned phenomena.

Spaces with nontrivial topologies provide quantum systems unprecedented properties [1–7]. As a prototypical space of a finite genus, the importance of a torus in modern physics is more far-reaching than applying periodic boundary conditions (PBC) in theoretical calculations. It plays a crucial role in quantum Hall physics. The ground state of a fractional quantum Hall state becomes degenerate on a torus or any surface with a finite genus [8]. Such degeneracy, which is unavailable on a cylinder or a flat space and defines the concept of the topological order lays the foundation of topological quantum computation [9]. However, due to the absence of magnetic monopoles in nature, it is impossible to generate a net magnetic flux through a closed surface in the real space. The study of quantum Hall states on a torus has eluded experiments so far.

Ultracold atoms provide physicists a unique platform to engineer Hamiltonians and allow physicists to achieve many quantum Hall states unattainable in electronic systems [10], such as quantum Hall states of bosons and quantum Hall states with high spins. Other than the typical harmonic potentials, ring traps have been implemented in an annular geometry [11, 12]. Linear and Laguerre-Gaussian (LG) Raman beams have been used to create spin-momentum coupling and spin-angular momentum coupling, respectively. [13–17]. If one considers the internal degree of freedom as a synthetic dimension, the spin-momentum coupling gives rise to a synthetic magnetic field in a two-dimensional plane [18, 19]. Whereas experiments have been focusing on open boundary conditions in the synthetic dimension [20, 21], there have been theoretical proposals on creating a periodic or twisted boundary condition [22–27]. However, few experiments has fulfilled the requirements of these proposals [28, 29].

We propose a simple scheme to realize a synthetic torus

penetrated by a net effective magnetic flux. Ultracold atoms confined in a ring trap in the real space are subjected to spin-angular momentum coupling induced by LG Raman beams. Either hyperfine spins or nuclear spins could be used to enable a cyclic coupling and form a loop in the discrete synthetic dimension. Cyclic couplings have been studied for different purposes, including realizing two-dimensional spin-orbit coupling and creating Yang monopoles [30–32]. Here, we use spin-angular momentum coupling to synthesize internal states and the real dimension into a synthetic Hall torus. PBCs in both the synthetic and the real dimension deliver a torus. Spin-angular momentum coupling produces finite effective magnetic fluxes penetrating its toroidal surface, signifying the rise of a synthetic Hall torus. Replacing Laguerre-Gaussian Raman beams by linear ones, our scheme applies to ordinary traps with open boundary conditions for creating synthetic Hall cylinders, which have been realized by experiments recently [28, 29].

We further unfold unique properties of synthetic Hall tori and cylinders. Unlike previous works including optical lattices in the real dimension [20, 21, 24, 26–28], we consider a continuous real space trap. Interestingly, periodic or quasiperiodic lattices emerge in the continuous real dimension, as a result of PBC in the synthetic dimension. The periodic lattice modulates the density of atoms with a fractionalized periodicity of the Hamiltonian and a unique band structure shows up. Energy bands form clusters with nonsymmorphic-symmetry-protected band crossings in each cluster. Wavepackets in each cluster swap with each other in Bloch oscillations. Though each single synthetic Hall torus or cylinder supports only extend states, once two of them are glued together, quasiperiodic lattices may emerge and lead to localized states in the real space. Such “localization from gluing” demonstrates the power of synthetic Hall tori or cylinders

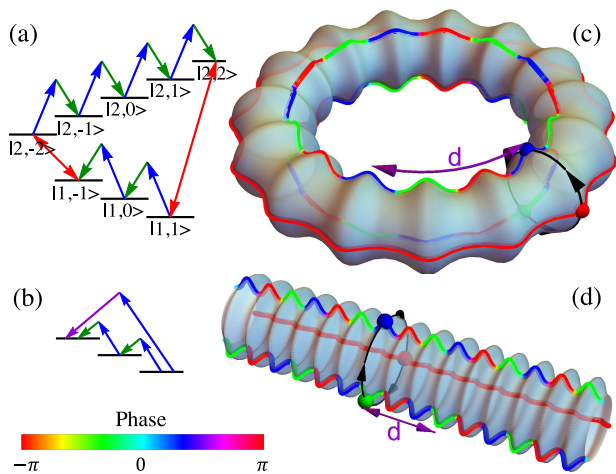


FIG. 1. (Color online) (a) Energy diagram for the hyperfine states and the laser coupling scheme. Blue and green arrows represent the Raman coupling. Bidirectional arrows represent microwave couplings. (b) Simplified coupling diagram for three internal states coupled by Raman beams. (c-d) Torus (Cylinder) formed by cyclically coupled three internal states in a real space ring trap. The density oscillation is depicted as the fluctuation of the radius of the torus or cylinder. Colored curves represent phases of the wavefunction of each spin component.

in accessing even more complex synthetic spaces and intriguing quantum phenomena there.

Proposed scheme and Hamiltonian. We consider M internal states in a real space ring trap. For alkali atoms, these M spins involves both $F = 1$ and $F = 2$, as shown in Fig. 1(a). At weak magnetic fields, linear Zeeman splitting dominates, thus a single pair of LG Raman beams simultaneously couples every consecutive states within each manifold; Microwave fields couple $|1, 1\rangle$ ($|1, -1\rangle$) and $|2, 2\rangle$ ($|2, -2\rangle$). These eight states form a circle in the synthetic dimension. Due to the opposite g factors between $F = 1$ and $F = 2$, a finite angular momentum transfer occurs once an atom finishes the loop in the synthetic dimension. A net effective magnetic flux emerges on the torus. Each hyperfine spin state has multiple angular momenta.

The number of internal states are controllable. On the one hand, at large magnetic fields, quadratic Zeeman splittings become important, and fewer spins can be separated out from the rest to form a smaller circle [26, 28–30, 32]. Note that shrinking the synthetic dimension does not change any results qualitatively, as fractional quantum Hall states can be adiabatically connected to 1D charge-density waves [33]. Chiral edge currents in the quantum Hall strips have also been observed using only three internal states [20, 21]. On the other hand, using the 1S_0 and 3P_0 states of Sr87 [34], one could cyclically couple up to 20 internal states.

Here, we consider nearest neighbors in the synthetic dimension coupled by LG Raman beams. The spin flip

from the j th spin state to the $j + 1$ th one is thus accompanied by an angular momentum increase $m_{j,j+1}$, which is the difference between the angular momenta carried by the two LG beams. A microwave coupling then corresponds to $m_{j,j+1} = 0$.

We define the position $x = \phi L / (2\pi)$ and the momentum $p = 2\pi m / L$, where ϕ is the azimuthal angle and L is the circumference of the real space ring. We also define $q_{j,j+1} = 2\pi m_{j,j+1} / L$ as the “momentum” transfer along the azimuthal direction. The advantage of the notation is that all results directly apply to a cylinder. In both the cylinder and the torus, x represents the direction in the real dimension. The Hamiltonian reads

$$H = \sum_{j=1}^M |\psi^j(x)\rangle \left(-\frac{\hbar^2}{2m_0} \partial_x^2 + \epsilon_j \right) \langle \psi^j(x)| + \sum_{j=1}^M \left(\Omega_{j,j+1} e^{iq_{j,j+1}x} |\psi^{j+1}(x)\rangle \langle \psi^j(x)| + h.c. \right), \quad (1)$$

where $\psi^j(x)$ denote the spacial wave function for the j th spin, ϵ_j the one (two) photon detuning in the microwave (Raman) transition, $\Omega_{j,j+1}$ the coupling strength between the j th and the $j + 1$ th spin state, and $\psi^{M+1}(x) = \psi^1(x)$. Whereas our results are very general and do not require tuning every single parameter arbitrarily, quadratic Zeeman splitting could create uneven energy separations and each pair of hyperfine spin states could be coupled by different lasers. Thus, $\Omega_{j,j+1}$ can be, in principle, tuned independently. The total phase accumulated after an atom finishes a circle $j \rightarrow j+1 \rightarrow j+2 \dots \rightarrow j-1 \rightarrow j$, $\varphi(x) \equiv e^{iQx}$ is finite and spatially dependent, where $Q \equiv \sum_{j=1}^M q_{j,j+1}$. The total synthetic magnetic flux on the surface of the torus per unit length in the physical dimension is then proportional to Q .

Nonsymmorphic symmetry and band structures. We start from commensurate momentum transfers, i.e., $q_{j,j+1} = n_j q_L$, where n_j are integers. For any coupling strengths $\Omega_{j,j+1}$, the reciprocal lattice vector q_L determines the periodicity of $H(x)$, $H(x) = H(x + \frac{2\pi}{q_L})$. If one of these couplings vanishes, the phases, $e^{iq_{j,j+1}x}$, can be absorbed to $|\psi^{j+1}(x)\rangle$, and any spin component in an eigenstate contains a single plane wave. In contrast, when all $\Omega_{j,j+1} \neq 0$, the phases cannot be gauged away under such PBC. A single spin component in any eigenstate contains multiple plane waves and the densities form standing waves. The lattice in the real space is therefore an emergent one from the PBC in the synthetic dimension.

The Bloch wavefunctions $\vec{\psi}_k(x)$ are simultaneous eigenstates of H and $\hat{T}(d)$ [$\hat{T}(d) \vec{\psi}_k(x) = e^{ikd} \vec{\psi}_k(x)$], where $\vec{\psi}(x)$ is a M -component wavefunction, k the quasi-momentum, and $d \equiv \frac{2\pi}{q_L}$ the lattice spacing, $T(d)$ the translation operator of distance d . We define the nonsymmorphic symmetry operator \hat{G} as a combination of

a translation for a fraction of the lattice space $T(2\pi/Q)$ in the real dimension and a unitary transformation U_s in the synthetic direction,

$$x \rightarrow x + \frac{2\pi}{Q}, \quad |\psi^{j>1}\rangle \rightarrow e^{-i\frac{2\pi}{Q} \sum_{j'=1}^{j-1} q_{j',j'+1}} |\psi^j\rangle. \quad (2)$$

Again, it is understood that $M+1$ is equivalent to 1. A simple example of the nonsymmorphic symmetry is the glide-reflection symmetry, a translation for half of the lattice spacing combined with a reflection in the perpendicular direction, which has played an important role in topological quantum matters [35–37]. Consider a special case, $\epsilon_j = 0$, $\Omega_{j,j+1} = \bar{\Omega}$ and $n_j = \bar{n}$, the synthetic dimension becomes translational invariant in the real dimension. \hat{G} and its multiples, together with the translation in the synthetic dimension, then form the conventional magnetic translation group [38]. In generic cases where the synthetic dimension does not have translation invariance, i.e., nonuniform ϵ_j , $\Omega_{j,j+1}$ or n_j . $[H, \hat{G}] = 0$ is still satisfied and signifies a nonsymmorphic symmetry.

We define $n \equiv Q/q_L = \sum_{j=1}^M n_j$. Many physical quantities depend on n , i.e., properties of the system crucially rely on how the synthetic magnetic field is distributed on the surface of the torus, not just the total flux. Applying \hat{G} for n times is equivalent to a translation in the physical dimension for one lattice spacing, $\hat{G}^n \psi_k(x) = e^{ikd} \psi_k(x)$. Thus,

$$\hat{G} \vec{\psi}_k(x) = c_s \vec{\psi}_k(x), \quad c_s = e^{i(\frac{kd}{n} + \frac{2s\pi}{n})}, \quad (3)$$

where $s = 1, 2, \dots, n-1, n$. Equation (3) shows that, as the quasimomentum k changes by a reciprocal lattice vector q_L , the eigenvalue of \hat{G} changes by $e^{2i\pi/n}$, i.e., the s th eigenvalue becomes the $s+1$ one. Meanwhile, $\vec{\psi}_k(x) = \vec{\psi}_{k+q}(x)$ is satisfied. Thus, we conclude that bands must form clusters, each of which contains n bands. These n bands are the n eigenstates of the operator \hat{G} with the s th eigenvalue c_s , and intersect with each other within the Brillouin zone (BZ).

We solve H in Eq. (1) using plane-wave expansions. The band structure fully agrees with the prediction from the above symmetry considerations. Fig. 2(a) shows the energy bands when $M = 3$, $q_{1,2} = q_{2,3} = q_{3,1} = q$, and coupling strength $\Omega_{1,2} = 1.2E_R$, $\Omega_{2,3} = 1.8E_R$, and $\Omega_{3,1} = 1.5E_R$, where $E_R = \hbar^2 Q^2 / 2m_0$ is the recoil energy defined by Q . Here, the reciprocal lattice vector $q_L = q$ and $n = Q/q_L = 3$. The cylindrical or toroidal surface is penetrated by a uniform flux. Thus, three bands exist in each cluster. The eigenstate of the s th band is

$$\begin{aligned} \vec{\psi}_k(x) &= e^{i(k+sq)x} (u_k^1(x), u_k^2(x), u_k^3(x))^T, \\ u_k^j(x) &= e^{i(j-1)qx} \sum_{l=-\infty}^{\infty} c_l^j(k) e^{ilQx}, \end{aligned} \quad (4)$$

where $u_k^j(x)$ is the periodic Bloch wavefunction of the j th spin state, l an integer, and $c_l^j(k)$ determined by Eq. (1).

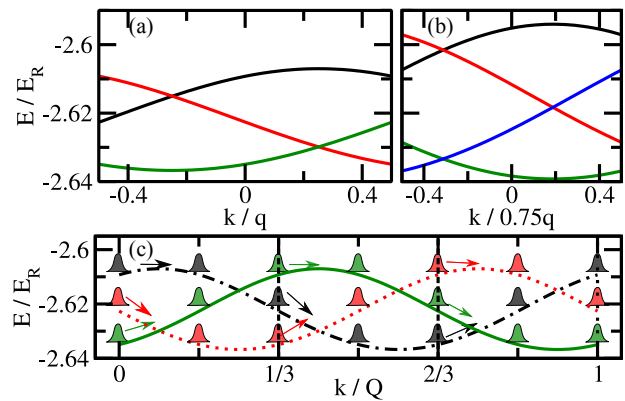


FIG. 2. Band structures when $q_{1,2} : q_{2,3} : q_{3,1} = 1 : 1 : 1$ (a) and $q_{1,2} : q_{2,3} : q_{3,1} = 1 : 1 : 2$ (b). (c): Bloch oscillation for (a). Vertical lines represent the boundaries of BZ.

The density of the j th spin state, $\rho_k^j(x) \equiv |u_k^j(x)|^2$ satisfies

$$\rho_k^j(x) = \rho_k^j(x + \frac{2\pi}{Q}) = \rho_k^j(x + \frac{d}{3}). \quad (5)$$

The total density $\rho(x) = \sum_j \rho_k^j(x)$, by definition, also satisfy Eq. (5) [39]. Despite the continuous real dimension, the density of atoms oscillates with a period only $1/3$ of that of the Hamiltonian, as shown in Fig. 1(c-d). In contrast, the relative phase between $u_k^2(x)$ [$u_k^3(x)$] and $u_k^1(x)$ has a periodicity of d , as shown by the colored curves in Fig. 1(c-d). As previously discussed, such results crucially depend on the PBC. Both periodic density and phase oscillations vanish once the synthetic dimension has an open boundary condition.

Swapping wave packets in Bloch oscillations. When a constant force is applied, a wavepacket in the momentum space experiences a Bloch oscillation, which has exactly the same period of the Hamiltonian in an ordinary band structure. In contrast, the period of the Bloch oscillation here is given by $3q$, tripling the reciprocal lattice vector. Due to the presence of band crossings, a wavepacket does not return to the original band after the momentum changes by q . Instead, it swaps with another wavepacket from a different band.

The significance of such Bloch oscillations here is that it traces the Wilson lines, a path-ordered integral of non-abelian Berry connections in the momentum space [40, 41]. Due to the nonsymmorphic-symmetry-protected band crossings, abelian Berry connections no longer applies when studying topological properties of the band structure. Non-abelian Berry connections and the Wilson lines characterize how a quantum state changes to a different one while the Hamiltonian returns to the original one [42, 43], a prototypical non-abelian operation. This is precisely what we see from Fig. 2(c). If we label the bands as 1, 2, 3 from bottom to top based on the energies, the green wave packet initially at band-1 moves to

band-3, meanwhile the red (black) one initially at band-2 (band-3) moves to band-1 (band-2) when $\Delta k = q$ [44]. When $\Delta k = Q = 3q$, these three wave packets swap with each other for six times, as shown in Fig. 2(c).

The above discussions can be directly generalized to other choices of $\{q_{j,j+1}\}$. If $q_{1,2} = q_{2,3} = \frac{3}{4}q$, $q_{3,1} = \frac{3}{2}q$, though the total momentum transferred, Q , is still $3q$, the same as the previously discussed case, q_L becomes $3q/4$ and $n = 4$. One thirds of the surface has a larger magnetic flux than the remaining region [44], and a cluster consists of four bands [Fig. 2(b)]. Changing the value of some of the wavevectors is equivalent to redistributing the magnetic flux on the surface, and leads to distinct band structures. We emphasize that the total number of states of the system remains unchanged. The change of the number of bands is associated with the change of BZ. In this example, the reciprocal lattice vector q'_L become $\frac{3}{4}q$. Shrinking the size of BZ then leads to an increase of the number of bands in a cluster.

Quasiperiodic lattices. If $q_{j,j+1}$ are incommensurate, e.g., $q_{1,2} : q_{2,3} : \dots : q_{M,1} = 1 : 1 : \dots : \gamma$, where $\gamma = \frac{\sqrt{5}-1}{2}$, a peculiar quasiperiodic lattice arises: certain quantities have well defined periodicities but others do not. For example, Eq. (4-4) holds for a generic $\{q_{j,j+1}\}$ when $M = 3$. Though H in Eq. (1) is aperiodic, the density of each spin still satisfies $\rho_k^j(x) = \rho_k^j(x + \frac{2\pi}{Q})$. The wavefunction of each spin component is still extended, as its plane wave expansion only includes multiples of Q . In contrast, the relative phases between different spin component are spatially variant and are not commensurate. Thus, the wavefunction $\psi_k(x)$ is aperiodic in the real dimension. Defining a pseudospin-1, $S_\mu = \sum_{j,j'} u_k^{j*}(x) \mathcal{F}_\mu^{j,j'} u_k^j(x)$, where $j, j' = 1, 2, 3$, $\mathcal{F}_\mu^{j,j'}$ are the spin-1 Pauli matrices, and $\mu = x, y, z$. $S_z(x)$ is periodic, $S_z(x) = S_z(x + 2\pi/Q)$, but $S_x(x)$ and $S_y(x)$ do not have well defined periods, as shown in Fig. 3(a).

On a cylinder, there is no restriction on the choice of $q_{j,j+1}$. In contrast, an irrational ratio $q_{j,j+1}/q_{j',j'+1}$ is not allowed on a torus, as the PBC in the real dimension require that all momentum scales are multiples of $2\pi/L$. Nevertheless, any irrational number can be approached by the ratio of two integers with increasing the integers' values. For instance, γ can be approximated by $\gamma_\alpha = a_{\alpha-1}/a_\alpha$, where $\{a_\alpha\}$ is the Fibonacci series 1,1,2,3,5, ..., with increased accuracy. When the approximation order α increases, the periodicity of $S_{x,y}(x)$ increases. γ_α with a small α well reproduces the result for a small x and a large γ .

Localization by gluing. Our scheme can be implemented to access more complex synthetic spaces. For instance, adding extra couplings to the synthetic dimension is equivalent to gluing multiple tori or cylinders. Figure 3(b) shows that two tori or cylinders with $M = 3$ can be glued to a single one with $M = 4$. In the real space, it is difficult to realize such gluing, as it is required

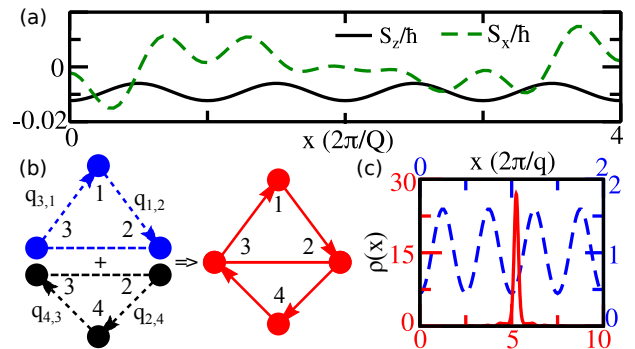


FIG. 3. (a) Spin polarization along the x and z direction as a function of x . (b) Schematic of the cross sections of two tori or cylinders when they are glued together. (c) Total density of the ground eigenstate at zero quasimomentum before (dashed line, only the top blue torus or cylinder is shown) and after (solid line) the gluing. $q_{1,2} = q_{3,1} = q$, $q_{2,3} = 0$, $q_{2,4} = q_{4,3} = \gamma q$, and all couplings $\Omega_{j,j'}$ are $2E_r$, where $E_r = \hbar^2 q^2 / 2m_0$ is the recoil energy defined by q . $\gamma_8 = 13/21$ has been used as an approximation of $\gamma = (\sqrt{5} - 1)/2$.

to identify certain parts of two different objects. Using the synthetic dimension, adding an additional tunneling through the interior of single tori or cylinder with $M = 4$, $\Omega' = \Omega_{2,3}$, immediately realizes this gluing and delivers a system with a different topology. Though each single torus or cylinder supports only extended eigenstates, after gluing them together, eigenstates at low energies could become localized, as shown in Fig. 3(c) [45]. The wavefunction of a single spin component now includes multiple momentum scales, $q_{1,2}$, and $q_{4,3}$, unlike a single torus or cylinder case where only Q is relevant. The interference of plane waves with incommensurate wave vectors could thus potentially localize the wavefunction.

To quantitatively characterizes the localization, we compute the width of the lowest band as a function of Ω' . It has been shown that the ground band width scales with a_α^{-2} for extended states, and decays much faster for localized states [46, 47]. Here, the scaled band width almost vanish at an intermediate value of Ω' , where eigenstates are localized, as shown in Fig. 4. When Ω' is very small, the wavefunction is still extended, similar to a single torus without Ω' . For large Ω' , dominating contributions to the wavefunction come from only two hyperfine spin states [2 and 3 in Fig. 3(b)] such that the incommensurate wave vectors are no longer relevant and the wavefunction is still extended.

The localization can also be characterized by the expansion of an initially localized wavepacket with a width σ_0 in the real space. We consider a Gaussian wave packet as the initial state. For small or large Ω' , where the eigenstates at low energies are delocalized, the width of the wave packet, σ , increases quickly. In contrast, σ grows much slower in the localized regime. To further consider interaction effects, we numerically solve a time-

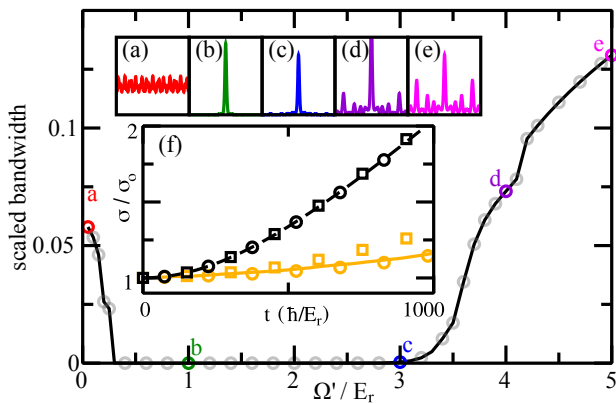


FIG. 4. Bandwidth multiplied by a_α^2/E_r as a function of Ω' for $\alpha = 12$. The inset (a), ..., (e) show the corresponding zero quasi-momentum ground state at $\Omega'/E_r = 0.05, 1, 3, 4, 5$, respectively with $\alpha = 8$. (f) The width of the Gaussian wave packet as a function of time. The solid orange (black dashed) curve represents non-interacting results for $\Omega' = 2E_r$ ($\Omega' = 0$). Squares and circles represent results for $\int g\rho_i^2 dx = \pm 0.003E_r$, respectively, where ρ_i is the density for the initial state.

dependent Gross-Pitaevskii equation,

$$i\hbar \frac{\partial \vec{\psi}(x)}{\partial t} = (\hat{H} + g\rho)\vec{\psi}(x), \quad (6)$$

where g is the interaction strength. We find that a weak repulsive (attractive) interaction slightly enhance (suppress) the dynamics. In addition, we have considered the ground state of interacting bosons in the trap. The main conclusions remain unchanged [44].

We have shown that atom-laser interactions allow physicists to synthesize Hall tori and cylinders hosting intriguing quantum phenomena in the emergent periodic and quasiperiodic lattices. We hope that our results will stimulate more works on synthetic spaces so as to explore physics that are not easy to access in conventional traps.

This work is supported by startup funds from Purdue University. Support by the National Science Foundation (NSF) through Grant No. PHY-1806796 is gratefully acknowledged.

[1] H. Kleinert, *Gauge Fields in Condensed Matter* (WORLD SCIENTIFIC, 1989).
 [2] C. Schulte, Quantum Mechanics on the Torus, Klein Bottle and Projective Sphere, in *Symmetries Sci. IX* (Springer US, Boston, MA, 1997) pp. 313–323.
 [3] K. Kaneda and Y. Okabe, Finite-size scaling for the Ising model on the Möbius strip and the Klein bottle, *Phys. Rev. Lett.* **86**, 2134 (2001).
 [4] W. T. Lu and F. Y. Wu, Ising model on nonorientable surfaces: Exact solution for the Möbius strip and the Klein bottle, *Phys. Rev. E* **63**, 026107 (2001).

[5] A. M. Turner, V. Vitelli, and D. R. Nelson, Vortices on curved surfaces, *Rev. Mod. Phys.* **82**, 1301 (2010).
 [6] T.-L. Ho and B. Huang, Spinor Condensates on a Cylindrical Surface in Synthetic Gauge Fields, *Phys. Rev. Lett.* **115**, 155304 (2015).
 [7] N.-E. Guenther, P. Massignan, and A. L. Fetter, Quantized superfluid vortex dynamics on cylindrical surfaces and planar annuli, *Phys. Rev. A* **96**, 063608 (2017).
 [8] X. G. Wen and Q. Niu, Ground-state degeneracy of the fractional quantum Hall states in the presence of a random potential and on high-genus Riemann surfaces, *Phys. Rev. B* **41**, 9377 (1990).
 [9] A. Y. Kitaev, Fault-tolerant quantum computation by anyons, *Ann. Phys. (N. Y.)* **303**, 2 (2003).
 [10] I. Bloch, J. Dalibard, and W. Zwerger, Many-body physics with ultracold gases, *Rev. Mod. Phys.* **80**, 885 (2008).
 [11] O. Morizot, Y. Colombe, V. Lorent, H. Perrin, and B. M. Garraway, Ring trap for ultracold atoms, *Phys. Rev. A* **74**, 023617 (2006).
 [12] S. Eckel, J. G. Lee, F. Jendrzejewski, N. Murray, C. W. Clark, C. J. Lobb, W. D. Phillips, M. Edwards, and G. K. Campbell, Hysteresis in a quantized superfluid ‘atomtronic’ circuit, *Nature (London)* **506**, 200 (2014).
 [13] Y. J. Lin, K. Jiménez-García, and I. B. Spielman, Spin-orbit-coupled Bose-Einstein condensates, *Nature (London)* **471**, 83 (2011).
 [14] K. Sun, C. Qu, and C. Zhang, Spin-orbital-angular-momentum coupling in Bose-Einstein condensates, *Phys. Rev. A* **91**, 063627 (2015).
 [15] L. Chen, H. Pu, and Y. Zhang, Spin-orbital angular momentum coupling in a spin-1 Bose-Einstein condensate, *Phys. Rev. A* **93**, 013629 (2016).
 [16] H.-R. Chen, K.-Y. Lin, P.-K. Chen, N.-C. Chiu, J.-B. Wang, C.-A. Chen, P.-P. Huang, S.-K. Yip, Y. Kawaguchi, and Y.-J. Lin, Spin-Orbital-Angular-Momentum Coupled Bose-Einstein Condensates, *Phys. Rev. Lett.* **121**, 113204 (2018).
 [17] D. Zhang, T. Gao, P. Zou, L. Kong, R. Li, X. Shen, X.-L. Chen, S.-G. Peng, M. Zhan, H. Pu, and K. Jiang, Ground-State Phase Diagram of a Spin-Orbital-Angular-Momentum Coupled Bose-Einstein Condensate, *Phys. Rev. Lett.* **122**, 110402 (2019).
 [18] A. Celi, P. Massignan, J. Ruseckas, N. Goldman, I. B. Spielman, G. Juzeliūnas, and M. Lewenstein, Synthetic Gauge Fields in Synthetic Dimensions, *Phys. Rev. Lett.* **112**, 043001 (2014).
 [19] E. Anisimovas, M. Račiūnas, C. Sträter, A. Eckardt, I. B. Spielman, and G. Juzeliūnas, Semisynthetic zigzag optical lattice for ultracold bosons, *Phys. Rev. A* **94**, 063632 (2016).
 [20] B. K. Stuhl, H. I. Lu, L. M. Ayccock, D. Genkina, and I. B. Spielman, Visualizing edge states with an atomic Bose gas in the quantum Hall regime, *Science* **349**, 1514 (2015).
 [21] M. Mancini, G. Pagano, G. Cappellini, L. Livi, M. Rider, J. Catani, C. Sias, P. Zoller, M. Inguscio, M. Dalmonte, and L. Fallani, Observation of chiral edge states with neutral fermions in synthetic Hall ribbons, *Science* **349**, 1510 (2015).
 [22] F. Grusdt and M. Hönig, Realization of fractional Chern insulators in the thin-torus limit with ultracold bosons, *Phys. Rev. A* **90**, 053623 (2014).
 [23] O. Boada, A. Celi, J. Rodríguez-Laguna, J. I. Latorre,

- and M. Lewenstein, Quantum simulation of non-trivial topology, *New J. Phys.* **17**, 045007 (2015).
- [24] M. Łącki, H. Pichler, A. Sterdyniak, A. Lyras, V. E. Lembessis, O. Al-Dossary, J. C. Budich, and P. Zoller, Quantum Hall physics with cold atoms in cylindrical optical lattices, *Phys. Rev. A* **93**, 013604 (2016).
- [25] J. C. Budich, A. Elben, M. Łącki, A. Sterdyniak, M. A. Baranov, and P. Zoller, Coupled atomic wires in a synthetic magnetic field, *Phys. Rev. A* **95**, 043632 (2017).
- [26] L. Taddia, E. Cornfeld, D. Rossini, L. Mazza, E. Sela, and R. Fazio, Topological Fractional Pumping with Alkaline-Earth-Like Atoms in Synthetic Lattices, *Phys. Rev. Lett.* **118**, 230402 (2017).
- [27] H. Kim, G. Zhu, J. V. Porto, and M. Hafezi, Optical Lattice with Torus Topology, *Phys. Rev. Lett.* **121**, 133002 (2018).
- [28] J. H. Han, J. H. Kang, and Y.-i. Shin, Band Gap Closing in a Synthetic Hall Tube of Neutral Fermions, *Phys. Rev. Lett.* **122**, 065303 (2019).
- [29] C.-H. Li, Y. Yan, S. Choudhury, D. B. Blasing, Q. Zhou, and Y. P. Chen, A Bose-Einstein Condensate on a Synthetic Hall Cylinder, [arXiv:1809.02122](https://arxiv.org/abs/1809.02122).
- [30] D. L. Campbell, G. Juzeliūnas, and I. B. Spielman, Realistic Rashba and Dresselhaus spin-orbit coupling for neutral atoms, *Phys. Rev. A* **84**, 025602 (2011).
- [31] L. Huang, Z. Meng, P. Wang, P. Peng, S.-L. Zhang, L. Chen, D. Li, Q. Zhou, and J. Zhang, Experimental realization of two-dimensional synthetic spin-orbit coupling in ultracold Fermi gases, *Nat. Phys.* **12**, 540 (2016).
- [32] S. Sugawa, F. Salces-Carcoba, A. R. Perry, Y. Yue, and I. B. Spielman, Second Chern number of a quantum-simulated non-Abelian Yang monopole. *Science* **360**, 1429 (2018).
- [33] A. Seidel and D.-H. Lee, Abelian and Non-Abelian Hall Liquids and Charge-Density Wave: Quantum Number Fractionalization in One and Two Dimensions, *Phys. Rev. Lett.* **97**, 056804 (2006).
- [34] M. M. Boyd, T. Zelevinsky, A. D. Ludlow, S. M. Foreman, S. Blatt, T. Ido, and J. Ye, Optical Atomic Coherence at the 1-Second Time Scale, *Science* **314**, 1430 (2006).
- [35] K. Shiozaki, M. Sato, and K. Gomi, Z_2 topology in nonsymmorphic crystalline insulators: Möbius twist in surface states, *Phys. Rev. B* **91**, 155120 (2015).
- [36] C. Fang and L. Fu, New classes of three-dimensional topological crystalline insulators: Nonsymmorphic and magnetic, *Phys. Rev. B* **91**, 161105(R) (2015).
- [37] Q.-Z. Wang and C.-X. Liu, Topological nonsymmorphic crystalline superconductors, *Phys. Rev. B* **93**, 020505(R) (2016).
- [38] J. Zak, Magnetic translation group, *Phys. Rev.* **134**, A1602 (1964).
- [39] We normalize the wave function according to $\int_0^{2\pi} |\vec{\psi}(\phi)|^2 d\psi = 2\pi (\int_0^L |\vec{\psi}(\phi)|^2 dx = L)$ for the torus (cylinder), where L should be multiples of the period of the underlying Hamiltonian. Thus, the wave function and the density is dimensionless in both cases.
- [40] T. Li, L. Duca, M. Reitter, F. Grusdt, E. Demler, M. Endres, M. Schleier-Smith, I. Bloch, and U. Schneider, Bloch state tomography using Wilson lines. *Science* **352**, 1094 (2016).
- [41] S.-L. Zhang and Q. Zhou, Two-leg Su-Schrieffer-Heeger chain with glide reflection symmetry, *Phys. Rev. A* **95**, 061601(R) (2017).
- [42] F. Wilczek and A. Zee, Appearance of Gauge Structure in Simple Dynamical Systems, *Phys. Rev. Lett.* **52**, 2111 (1984).
- [43] M. Fruchart, Y. Zhou, and V. Vitelli, Dualities and non-Abelian mechanics, [arXiv:1904.07436](https://arxiv.org/abs/1904.07436).
- [44] See the supplemental materials at XXX for Bloch oscillation in the presence the band crossings, interaction effects on the expansion of Gaussian wave packet in the real space, expansion dynamics of the ground state in the harmonic trap, a realistic setup in experiments, and comparisons between the uniform and nonuniform flux.
- [45] Only half of the period is shown. Due to the inversion symmetry and nonsymmorphic symmetry, there are, in general, 2 or 4 peaks in a period, $2\pi a_s/q$. As the approximation order increase, the decrease of the width of the wavefunction is accompanied by the increase of the period and the separation between peaks.
- [46] H. Hiramoto and M. Kohmoto, Electronic Spectral and Wavefunction Properties of One-Dimensional Quasiperiodic Systems: A Scaling Approach, *Int. J. Mod. Phys. B* **06**, 281 (1992).
- [47] R. B. Diener, G. A. Georgakis, J. Zhong, M. Raizen, and Q. Niu, Transition between extended and localized states in a one-dimensional incommensurate optical lattice, *Phys. Rev. A* **64**, 033416 (2001).

Supplemental Material of “Emergent periodic and quasiperiodic lattices on surfaces of synthetic Hall tori and synthetic Hall cylinders”

The notation employed in this Supplemental Material follows that introduced in the main text. Section I used the non-abelian Wilson line technique to clarify why the crossing is avoided in Fig. 2 of the main text. Section II clarifies the parameters used in the simulation in Fig. 4 of the main text. Section III provides an alternative simulation: expansion of the ground state in a 1D harmonic trap. Section IV provides a full 3D simulation of a proposed experiment to demonstrate the localization of the ground state due to gluing of two cylinders. Section V clarifies Fig. 2(a-b) in the main text.

BLOCH OSCILLATIONS IN THE PRESENCE OF BAND CROSSINGS

In the presence of a constant force, F , the quasi-momentum becomes $k_f = k_0 + Ft$ at time t , where k_0 is the initial quasi-momentum at $t = 0$. In the adiabatic limit, the inter-band transition can be determined by the path-ordered integral [40, 41],

$$W(k_f; k_0) = \hat{P} \exp[i \int_{k_0}^{k_f} \hat{A}(k) dk / \hbar], \quad (\text{S1})$$

where \hat{P} is the path-ordering operator and the matrix representation of the non-Abelian Berry connection $\hat{A}(k)$ is defined as $A_{s',s}(k) = \langle \vec{u}_{s'k} | i \partial_k | \vec{u}_{sk} \rangle$, where $|\vec{u}_{sk}\rangle$ is the periodic Bloch wavefunction in the s th band,

$$|\vec{u}_{sk}\rangle = e^{isq_L x} \sum_{j=1}^M \sum_l \tilde{c}_{l,s}^j(k) e^{ilQx} |j\rangle. \quad (\text{S2})$$

We obtain

$$A_{s',s}(k) = \sum_j \sum_{l,l'}^M \left(\tilde{c}_{l',s'}^{j*}(k) \partial_k \tilde{c}_{l,s}^j(k) \right) \int_0^{2\pi/q_L} e^{i[(s-s')q_L + (l-l')Q]x} dx \sim \delta((s-s')q_L + (l-l')Q). \quad (\text{S3})$$

As $|s-s'|q_L \leq (n-1)q_L$ and $|l-l'|Q \geq nq_L$ (if $l \neq l'$), to ensure that $(s-s')q_L + (l-l')Q = 0$ is valid, $s = s'$ and $l = l'$ must be satisfied. Thus, $A_{s',s}(k) \sim \delta(s-s')$; Here, $n = Q/q_L$ is defined in the main text. This means that during the time evolution, there is no transition between bands with different s (different colored bands in Fig. 2 of the main text).

INTERACTION EFFECTS ON THE EXPANSION OF A GAUSSIAN WAVE PACKET IN THE REAL SPACE

As discussed in the main text, we consider a Gaussian wave packet as the initial state. All the spin components have equal amplitude and phase. The width of the wave packet, $\sigma_0 = \sqrt{\langle x^2 \rangle - \langle x \rangle^2}$, is $455/q$. We use $\gamma_8 = 13/21$ to approximate γ . The density spread σ_0 is roughly 3.5 times the underlying period of the Hamiltonian. Figure S1 shows the ratio of the width in a later time t to σ_0 , where $t = 1000\hbar/E_r$, as a function of the

initial interaction energy $E_i = \int g\rho_i^2 dx$ for $\Omega' = 0$ and $\Omega' = 2E_r$. In both cases, weak attractive (repulsive) interactions decrease (increase) the width, $\sigma(t)$. When interactions are strong enough, the width always increase with increasing the strengths of interactions due to the mixing with extended states at high energies.

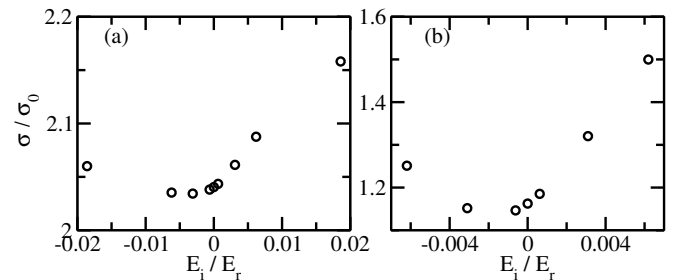


FIG. S1. Density spread as a function of initial interaction energy E_i for $\Omega' = 0$ (a) and $\Omega' = 2E_r$ (b).

EXPANSION DYNAMICS OF THE GROUND STATE IN A HARMONIC TRAP

We consider weakly interacting bosons in a harmonic trap with the trapping frequency $\omega = 0.034E_r/\hbar$, and use the imaginary time propagation to find the ground state. For non-interacting systems, the ground state has a Gaussian profile. In the presence of a weak repulsive interaction, the density is featured with a Thomas-Fermi profile.

Then we turn off the trap and the interactions, and let the cloud expand. Fig. S2 shows the width of the wavepacket as a function of time. When $\Omega' = 0$, the ground state in the trap is an extended one. Therefore, the wavepacket expands quickly after the trap and interactions are turned off. In contrast, when $\Omega' = 2E_r$, the ground state is a localized one. Even after turning off the trap and interaction, the width of the wavepacket has little changes, well reflecting the localized nature of the ground state in the trap. As a further comparison, we turn on a weak interaction in the expansion dynamics once the trap is turned off. It is clear that a weak repulsive interaction speeds up the expansion and a weak attractive interaction slows it down.

All these results are similar to those presented in the main text. It means that a shallow trap used in typical cold atom experiments do not change our qualitative results and main conclusions. In a shallow trap, though the momentum is no longer a good quantum number and an extended state does not extend to infinity, it can still spread over the whole trap. In contrast, localized states still remain localized, provided that the trapping potential is much smaller than the energy gap between the localized states and delocalized ones.

A REALISTIC SETUP IN EXPERIMENTS

Our scheme can be realized in laboratories as a simple generalization of some current experiments [29]. We choose four hyperfine states of ^{87}Rb , $|F, m_F\rangle = |2, 2\rangle, |2, 1\rangle, |1, 0\rangle, |1, 1\rangle$. States $|2, 2\rangle$ and $|2, 1\rangle$ are resonantly coupled by one pair of counter propagating Raman beams with recoil momentum $k_r = 2\pi/\lambda$, where $\lambda = 790\text{nm}$ is the wavelength. The momentum transferred is $2k_r$. States $|1, 0\rangle$ and $|1, 1\rangle$ are resonantly coupled by another pair of Raman beams with the same wavelength that is tilted with a small angle θ with respect to the first pair of Raman beams. The momentum transferred is $2k_r \cos\theta$, where the angle θ is chosen such that $\cos\theta$ is irrational or rational, say, $\cos\theta = \gamma_i$, where γ_i is defined in the main text. One microwave couples states $|2, 2\rangle$ and $|1, 1\rangle$, and another couples states $|2, 1\rangle$ and $|1, 0\rangle$. This completes a cyclic coupling between four states and delivers a synthetic cylinder. Replacing Raman beams by LG beams, this creates a synthetic torus.

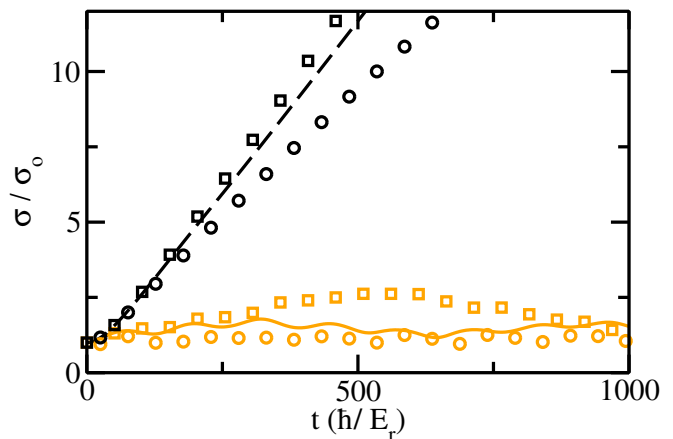


FIG. S2. The evolution of the wavepacket after releasing from the trap. The solid orange (black dashed) curve represents results for $\Omega' = 2E_r$ ($\Omega' = 0$) when the interaction is also turned off in the expansion. Squares and circles represent results for a small repulsion and a small attractive interaction added in the expansion, respectively. The absolute interaction strength, $|g|$, is the same, and the interaction energies $E_i = \int g\rho_i^2 dx$ differ because of different densities. For $\Omega' = 2E_r$, $E_i/E_r \approx 0.010$ and -0.039 for positive and negative g , respectively. For $\Omega' = 0$, $E_i/E_r \approx 0.0098$ and -0.013 for positive and negative g , respectively.

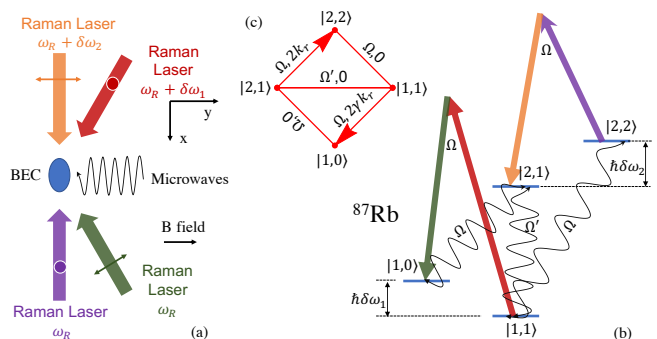


FIG. S3. (a) A Bose-Einstein Condensate is confined in a harmonic trap. Straight arrows represent Raman lasers and wiggles indicate microwaves. (b) A scheme to couple hyperfine states of ^{87}Rb . Four states are cyclically coupled by pairs of Raman lasers (arrows) and microwaves (wiggles). In addition, a microwave couples states $|1, 1\rangle$ and $|2, 1\rangle$ with coupling strength Ω' . (c) A schematic of the cross sections of two cylinders or tori when they are glued together. The coupling strengths and momenta transferred are labeled.

All coupling strengths are scaled with $2E_r = \hbar^2(2k_r)^2/m$, where m is the mass of a Rubidium atom. As discussed in the main text, eigenstates are extended, even when $\cos\theta$ is irrational and the Hamiltonian is quasi-periodic.

To glue two cylinders or tori, an extra microwave coupling between states $|2, 1\rangle$ and $|1, 1\rangle$ could be added. The coupling strength is Ω' . The experimental setup is depicted in Fig. S3.

Using realistic experimental parameters, we perform time-dependent simulations using the Gross-Pitaevskii equation. We consider 15000 ^{87}Rb atoms in a three-dimensional harmonic trap with an angular trapping frequency $2\pi \times 500\text{Hz}$. We compute the ground states in the presence of Raman and microwave couplings, interactions and the harmonic trap. After the initial state is prepared, we turn off the trap along \hat{x} , the direction of momentum transfer. The transverse confinement remains. All the inter- and intra-species scattering lengths are well approximated by $93a_0$, where a_0 is the Bohr radius. The angle is chosen such that $\cos\theta = 13/21$.

Fig. S4 shows the width of the wavepacket, σ , as a function of time t after the trap and the interaction are turned off. The wavepacket expands fast when $\Omega' = 0$, as a consequence of the extended ground state in the trap. It expands little when $\Omega' = 2E_r$, reflecting the localized nature of the initial state in the trap after glueing two cylinders.

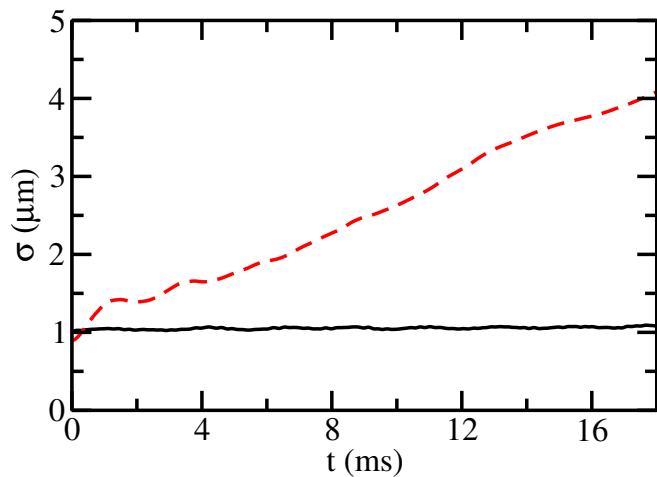


FIG. S4. Expansion dynamics when the ground state is released from the trap along the x direction. Solid line and dashed lines represent results of $\Omega' = 2E_r$ and $\Omega' = 0$, respectively.

COMPARISONS BETWEEN THE UNIFORM AND NONUNIFORM FLUX

The ground states of the systems for Fig. 2(a) and Fig. 2(b) in the main text are depicted in Fig. S5(a). The density modulation of each spin component is de-

termined by the total momentum Q , or equivalently, the total flux penetrating a unit length. The period of the density oscillation $\bar{d} = 2\pi/Q$. However, the relative phases between different spin components depend on how the flux is distributed on the surface. For the system in Fig. 2(a), $n = 3$, $q_L = q = Q/3$, and the flux is uniformly distributed. The relative phase has a period of $d = 2\pi/q = 3\bar{d}$. The lattice spacing is therefore

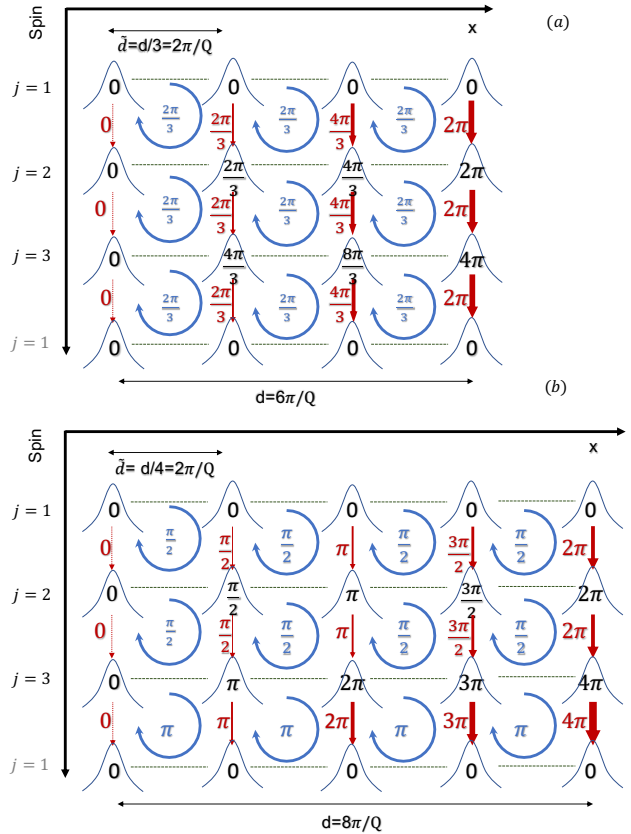


FIG. S5. Curves represent the density profiles of each individual spin component near the maxima. The phases of the wavefunctions are also shown. Red arrows represent the spatially dependent coupling along the synthetic direction. Maxima of the density form plaquettes, in which the flux per plaquette are shown.

$d = 6\pi/Q$. In contrast, for the system in Fig. 2(b), $n = 4$, $q_L = 3q/4$, and the distribution of the flux is nonuniform. The relative phase has a period of $8\pi/Q$, and the lattice spacing is therefore $8\pi/Q$.